Evaluation of Material Integrity Using Reduced Order Computational Methodology

Dr. H.T. Banks
Center for Research in Scientific Computation
North Carolina State University

Michele L. Joyner
Center for Research in Scientific Computation
North Carolina State University

Buzz Wincheski
NASA Langley Research Center

Dr. William P. Winfree
NASA Langley Research Center

Report Documentation Page

Form Approved
OMB No. 0704-0188

1. REPORT DATE	2. REPORT TYPE	3. DATES COVERED
1999		**00-00-1999 to 00-00-1999**

4. TITLE AND SUBTITLE	5a. CONTRACT NUMBER
Evaluation of Material Integrity Using Reduced Order Computational Methodology	5b. GRANT NUMBER
	5c. PROGRAM ELEMENT NUMBER
6. AUTHOR(S)	5d. PROJECT NUMBER
	5e. TASK NUMBER
	5f. WORK UNIT NUMBER
7. PERFORMING ORGANIZATION NAME(S) AND ADDRESS(ES) **North Carolina State University,Center for Research in Scientific Computation,Raleigh,NC,27695-8205**	8. PERFORMING ORGANIZATION REPORT NUMBER
9. SPONSORING/MONITORING AGENCY NAME(S) AND ADDRESS(ES)	10. SPONSOR/MONITOR'S ACRONYM(S)
	11. SPONSOR/MONITOR'S REPORT NUMBER(S)

12. DISTRIBUTION/AVAILABILITY STATEMENT
Approved for public release; distribution unlimited

13. SUPPLEMENTARY NOTES

14. ABSTRACT
see report

15. SUBJECT TERMS

16. SECURITY CLASSIFICATION OF:			17. LIMITATION OF ABSTRACT	18. NUMBER OF PAGES	19a. NAME OF RESPONSIBLE PERSON
a. REPORT **unclassified**	b. ABSTRACT **unclassified**	c. THIS PAGE **unclassified**		**58**	

Abstract

This paper explores the feasibility of detecting damage within structures such as air foils by application of eddy current based techniques and reduced order modeling. To identify the geometry of a damage, an optimization algorithm is employed which requires solving the forward problem numerous times. Therefore, the forward algorithm must be solved with extremely fast and accurate solution methods. In constructing these forward methods, we employ reduced order Proper Orthogonal Decomposition (POD) techniques.

The POD technique is a method which creates an "optimal" ordered basis in the sense that information captured in the first few basis elements is maximized. One then uses a fixed number (based on a quantitative formula for percentage energy captured) of the first few basis elements, called the reduced POD basis, in the forward algorithm. Since one uses only a small number of basis elements, one is able to create a fast forward algorithm that accurately represents the relevant information.

In this paper, for illustrative purposes and proof-of-concept, we consider rectangular "cracks" parameterized by a vector parameter $\mathbf{q}$ representing the length, thickness, depth, center, etc. of the damage. We attempt to recapture the parameters of a damage assuming we have access to the magnetic vector potential $\mathbf{A}$ (which is not pratical experimentally) or the magnetic flux density $\mathbf{B}$. Our analysis uses simulated data $\hat{\mathbf{A}}$ or $\hat{\mathbf{B}}$ with normally distributed noise to represent corrupted experimental data. When recapturing the length or thickness of a damage using the component of the magnetic flux density orthogonal to the eddy current flow in the sample, the methods are shown to be efficient and robust even with data containing 10% relative noise.

1 Introduction and Problem Formulation

In the field of nondestructive evaluation, new and improved techniques are constantly being sought to facilitate the detection of hidden corrosion and flaws in structures such as air foils and pipelines. Many electromagnetic techniques and instruments already exist to aid in the detection of hidden flaws and corrosion. Some of the devices and techniques in use today involve the magneto-optic/eddy current imager [8, 24] in conjunction with eddy current imaging [9, 10], the self-nulling eddy current probe [26] along with conformal mapping techniques [27], and the SQUID (Superconducting Quantum Interference Device) through the use of either injected current methods or induced eddy current methods [5, 7, 12, 21, 23, 25]. We attempt to contribute to these techniques already in use by decreasing the computational time required to detect and characterize a damage in a material explicitly. In other words, given data obtained from a measuring device, we seek to locate and parameterize the damage while minimizing the amount of time required to complete this task. To this end, we formulate and develop a problem complete with computational methods and results.

The proposed computational approach is based on approximation ideas from the Karhunan-Loeve or Proper Orthogonal Decomposition reduced order methodology. Recently these techniques have been successfully used in reduced order methodologies for feedback control design [1, 6, 14] as well as open loop control design [20]. Here we propose for the first time the use of such techniques in electromagnetic based damage detection problems. Initial findings reported below are most encouraging.

1.1 Description of Problem

Depending upon the application, different measuring devices and techniques are used in nondestructive evaluation. An advanced method of damage detection uses a device such as the SQUID or self-nulling probe as the sensor for eddy current methods. One way in which the eddy current method is implemented is by placing a thin conducting sheet carrying a uniform current above or below the sample. The current within the sheet induces a magnetic field perpendicular to it that produces a current within the sample, called an eddy current. When a flaw is present within the sample, the flaw disrupts the eddy current flow near the flaw and this disturbance is manifested in the magnetic field detected by the measuring device. Using these measurements of the magnetic field, we attempt to reconstruct the geometry and location of the flaw explicitly.

To test the feasibility of reconstructing the geometry of the damage, we consider a two-dimensional problem in which the damage (which we shall refer to as a "crack") is rectangular in shape. In the two-dimensional problem, we assume we have uniformity in the direction of the current flow in the conducting sheet which we label the z direction, denoting the width of the sample. The x direction denotes the length of the sample while the y direction denotes the height or thickness of the sample. To further simplify the test problem, we disregard the boundary effects of the materials in the x direction (sample length) by assuming an infinite sample and conducting sheet in that direction. If the conducting sheet and sample are not of infinite extent, we have to take into account the discontinuities in the current flow at the boundaries. Because we are considering materials of infinite extent, we will construct our forward problem by focusing on a small "window". We will center this "window" such that the left boundary of the "window", at location $x = 0$, is positioned in the center of the crack in the x direction, i.e. the crack is symmetric around the yz plane at $x = 0$. Therefore, at both the left and right boundaries of the "window" we assume evenly symmetric boundary conditions to account for the symmetry of the crack as well as the infinite extent of the sample and conducting sheet in the x direction. A schematic of the resulting two-dimensional problem is depicted in Figure 1 where it is assumed that the sample (which is $20mm$ thick) is composed of aluminum and the conducting sheet (which is $0.1mm$ thick) is made up of copper.

Although certain simplifications are made in the two-dimensional case, the two-dimensional analysis is relevant to special three-dimensional cases. In a "true" three-dimensional case, the sample will be of finite length (finite in the x direction). However, if the crack is located "far enough" away from the boundaries of the sample in the x direction, we can assume the boundary effects are not sufficiently significant to effect the measurements taken by a SQUID (or similar device). Therefore, the infinite extent of the sample in the test problem will fairly accurately portray the finite sample in the three dimensional case. Similarly, in the two-dimensional test problem, we assume the sample along with the damage or crack to have an infinite width. However, in the three-dimensional case, the crack will have a finite width. To account for this, we assume that data will be taken by scanning along the length of the sample on a line fixed at a certain height and width using a SQUID. If the line upon which we are scanning is fixed in the z direction (along the width of the sample) so that the line is "far enough" away from the edges of the crack in the z direction (along the width of the crack), we should still be able to use the two-dimensional analysis to determine the

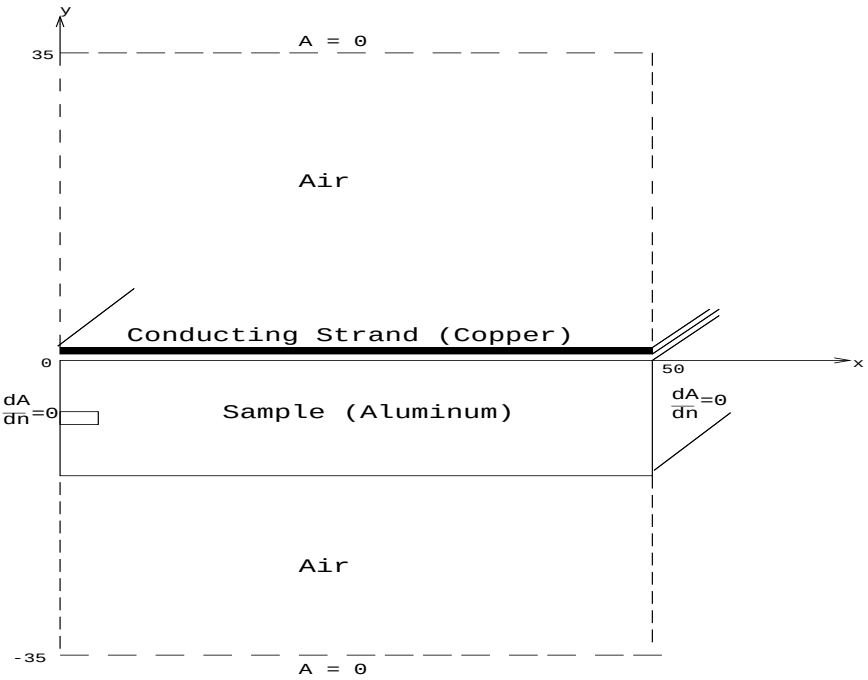

Figure 1: 2-D Schematic of Problem

feasibility of identifying length, thickness (or height) and depth of the crack with SQUID data.

1.2 The Use of Phasors

As mentioned in the previous section, a conducting sheet carrying a uniform current is placed above the sample to induce eddy currents within the sample. Without loss of generality, we assume the source current has the form

$$\overline{\mathbf{J}}_s = J_s cos(\omega t)\hat{\mathbf{k}} = J_s Re(e^{i\omega t})\hat{\mathbf{k}}.$$

This current produces a magnetic field $\overline{\mathbf{H}}(x, y, t)$ described by Maxwell's equations. At the surface of the sample, the magnetic field has the same time dependence as the source current,

$$\overline{\mathbf{H}}(x, y, t) = \tilde{\mathbf{H}}(x, y)cos(\omega t).$$

However, as the magnetic field penetrates into the sample, a phase lag results due to the finite cnductivity of the aluminum. In other words, the magnetic

field takes the form

$$\overline{\mathbf{H}}(x, y, t) = \tilde{\mathbf{H}}(x, y) cos(\omega t + \theta(x, y)),$$

where the term $\theta(x, y)$ takes into account the depth of penetration. Hence, $\tilde{\mathbf{H}}(x, y)$ is a vector field quantity which keeps track of the magnitude and direction of $\overline{\mathbf{H}}$ at each point in space while $\theta(x, y)$ denotes the phase shift from the original cosine wave at the same point in space. Consequently, the quantities of interest are $\tilde{\mathbf{H}}(x, y)$ and $\theta(x, y)$. To keep track of these quantities, denoting the magnitude, direction, and phase lag, we can use vector phasors.

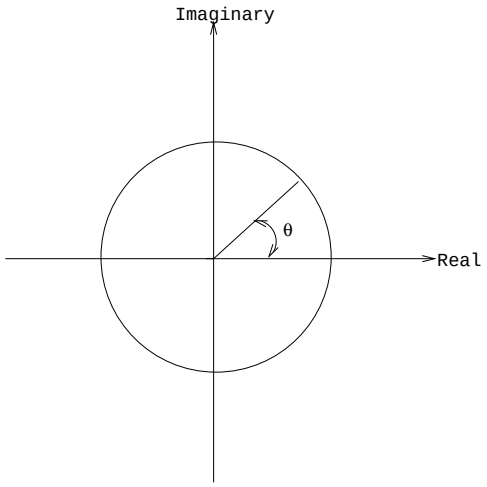

Figure 2: Illustration of Phasor Notation

A phasor [4, 22] is a complex quantity which completely defines the magnitude and phase shift for $\overline{\mathbf{H}}(x, y, t)$. Figure 2 illustrates how the magnitude and phase are defined through the complex number. The magnitude is represented by the radius of the circle, and the phase is the angle which the complex vector makes with the real axis. Thus, the vector phasor $\mathbf{H}$ and the explicit time dependent field $\overline{\mathbf{H}}(x, y, t)$ are related in the following way

$$\overline{\mathbf{H}}(x, y, t) = Re(\mathbf{H}(x, y) e^{i\omega t}) \tag{1}$$

in which all of the phase information and direction is captured in the complex vector phasor $\mathbf{H}$. For this reason, in the remainder of the paper we will assume no explicit time dependence in the fields examined, but instead consider the fields to be complex vector phasors, denoted $\mathbf{H}$, $\mathbf{B}$, etc, and

account for the time dependence of the fields through phase shifts contained in the phasors.

1.3 Formulation of Forward Problem

Maxwell's equations are the basis of the derivation in the forward problem. However, since we are expressing the various fields in terms of phasors which depend on space coordinates but not explicitly on time, we want to express time-dependent Maxwell's equations in terms of phasors. We first examine the explicit time-dependent Maxwell's equations. The usual system is written as

$$\nabla \cdot \overline{\mathbf{B}} = 0, \tag{2}$$

$$\nabla \cdot \overline{\mathbf{D}} = \rho, \tag{3}$$

$$\nabla \times \overline{\mathbf{E}} = -\frac{\partial}{\partial t}\overline{\mathbf{B}}, \tag{4}$$

and

$$\nabla \times \overline{\mathbf{H}} = \overline{\mathbf{J}} + \frac{\partial}{\partial t}\overline{\mathbf{D}}. \tag{5}$$

To examine the relationship between the explicit time-dependent Maxwell's equations and Maxwell's equations in terms of phasors, we examine the relationship in equation (1). Based upon this relationship, the time derivative for $\overline{\mathbf{H}}(x, y, t)$ (and similarly other fields) is given by

$$\frac{\partial}{\partial t}\overline{\mathbf{H}}(x, y, t) = i\omega Re(\mathbf{H}(x, y)e^{i\omega t}). \tag{6}$$

Substituting the appropriate form of equations (1) and (6) into equations (2) - (5), we obtain the phasor form of Maxwell's equations

$$\nabla \cdot \mathbf{B} = 0, \tag{7}$$

$$\nabla \cdot \mathbf{D} = \rho, \tag{8}$$

$$\nabla \times \mathbf{E} = -i\omega\mathbf{B}, \tag{9}$$

and

$$\nabla \times \mathbf{H} = \mathbf{J} + i\omega\mathbf{D}. \tag{10}$$

Thus equations (7) - (10) hold for our entire "window", denoted Ω.

We could further simplify equations (7) - (10) by making some observations. First of all, since our system is considered to be electrically neutral,

the internal electric charge density ρ equals zero. Secondly, by examining the conductivity σ of aluminum and copper and by using Ohm's law

$$\mathbf{J} = \sigma \mathbf{E},$$

we can argue $\mathbf{J} \approx 10^7 \mathbf{E}$. On the other hand, the constitutive law

$$\mathbf{D} = \epsilon \mathbf{E}, \tag{11}$$

indicates $\mathbf{D} \approx 10^{-11} \mathbf{E}$. We are using a frequency of $60Hz$ in our problem which yields an angular frequency of approximately $3 \times 10^2 rad/sec$, and thus $\omega \mathbf{D} \approx 10^{-9} \mathbf{E}$. Consequently, in the sample and conducting sheet $\mathbf{J} >> \omega \mathbf{D}$ which implies we could assume $\omega \mathbf{D} \approx 0$ in both the sample and conducting sheet in equation (10). In other words, the term $\omega \mathbf{D}$ on the right side of equation (10) is only significant in the air. Thus the form of Maxwell's equations we will use in the computations are given by

$$\nabla \cdot \mathbf{B} = 0, \tag{12}$$

$$\nabla \cdot \mathbf{D} = 0, \tag{13}$$

$$\nabla \times \mathbf{E} = -i\omega \mathbf{B}, \tag{14}$$

and

$$\nabla \times \mathbf{H} = \mathbf{J} + i\omega \mathbf{D} \tag{15}$$

where, as noted above, the term $i\omega \mathbf{D}$ is only significant in the air. However, we shall retain this term in all of Ω since this is done in the commercial simulator (Ansoft) that we employ below.

Based upon equation (12) and vector null identities, we can represent $\mathbf{B}$ as the curl of a vector potential $\mathbf{A}$, $\mathbf{B} = \nabla \times \mathbf{A}$, where $\mathbf{A}$ is referred to as the magnetic vector potential. The forward problem will be formulated in terms of this magnetic vector potential from which we can derive both the magnetic field $\mathbf{H}$ and magnetic flux density $\mathbf{B}$. Accordingly, we want to combine Maxwell's equations to obtain equations in conjunction with boundary conditions which completely determine the behavior of the magnetic vector potential $\mathbf{A}$ in Ω defined by

$$\Omega = \{(x, y, z) \in R^3 : 0mm \leq x \leq 50mm, -35mm \leq y \leq 35mm\}.$$

Using the identity $\mathbf{B} = \nabla \times \mathbf{A}$ in equation (14), we have

$$\nabla \times \mathbf{E} = -i\omega(\nabla \times \mathbf{A}) \quad \text{or} \quad \nabla \times (\mathbf{E} + i\omega \mathbf{A}) = 0.$$

Again using vector null identities, the cross product of $\mathbf{E} + i\omega\mathbf{A}$ being zero implies $\mathbf{E}+i\omega\mathbf{A}$ can be written as the gradient of a scalar potential, denoted by ϕ. As a result,

$$\mathbf{E} = -i\omega\mathbf{A} - \nabla\phi. \tag{16}$$

Finally, we can use equations (15) and (16) in conjunction with Ohm's law, the constitutive law given by (11) and the constitutive law $\mathbf{H} = \frac{1}{\mu}\mathbf{B}$, to obtain

$$\nabla \times \left(\frac{1}{\mu}\nabla \times \mathbf{A}\right) = \sigma(-i\omega\mathbf{A} - \nabla\phi) + i\omega\epsilon(-i\omega\mathbf{A} - \nabla\phi) \quad \forall x, y \in \Omega. \tag{17}$$

In the above equality, the right side represents the total current density $\mathbf{J}$ which is made up of the source current density, eddy current density and displacement current density. The source current density $\mathbf{J_s}$ is due to differences in electric potential; therefore, $\mathbf{J_s}$ is represented by the term $-\sigma\nabla\phi$. The term $-i\omega\sigma\mathbf{A}$ represents the eddy current density, $\mathbf{J_e}$, produced due to a time-varying magnetic field. Finally, the displacement current density, $\mathbf{J_d}$, due to time-varying electric fields is given by the term $i\omega\epsilon(-i\omega\mathbf{A} - \nabla\phi)$.

Since equation (17) contains two unknowns, $\mathbf{A}$ and ϕ, we need an additional equation to uniquely determine solutions of the system. In the literature [4, pp. 327-328],[11, pp.219-221] a "gauge" is commonly chosen which uniquely defines both $\mathbf{A}$ and ϕ. In time-varying problems a gauge satisfying the Lorentz condition

$$\nabla \cdot \mathbf{A} + \mu\epsilon\frac{\partial\phi}{\partial t}, \tag{18}$$

is most often imposed. However, based upon the geometry in our test problem, $\nabla \cdot \mathbf{A}$ can be seen to be zero. This follows since the only nonzero component of $\mathbf{A}$ is A_3, the component of $\mathbf{A}$ in the z direction (the direction of the current density $\mathbf{J}$). Therefore, $\nabla \cdot \mathbf{A} = \frac{\partial A_3}{\partial z} = 0$ since we have uniformity in the z direction. With $\nabla \cdot \mathbf{A} = 0$, imposing the Lorentz gauge in this problem would imply ϕ is constant in time. This is not a realistic assumption in this test problem since we have an alternating current. Instead we use the relationship

$$I = \int_{cs} \mathbf{J} \cdot \mathbf{n}da = \int_{cs} (\sigma(-i\omega\mathbf{A} - \nabla\phi) + i\omega\epsilon(-i\omega\mathbf{A} - \nabla\phi)) \cdot \mathbf{n}da \tag{19}$$

between the total current I flowing in the conducting sheet (cs) and the total current density $\mathbf{J}$ within the conducting sheet. This is the second equation used in the software package Ansoft Maxwell 2D Field Simulator

which we use in our computational efforts. Therefore, we have two coupled equations (17) and (19) in which the magnetic vector potential $\mathbf{A}$ can be uniquely determined if appropriate boundary conditions are specified. We remark that the usual imposition of a Lorentz gauge decouples the equations for the potentials $\mathbf{A}$ and ϕ [11, p.220]. Since we are following the Ansoft formulation, we do not do this here.

Recall, from Section 1.1 that we assume evenly symmetric x boundaries due to the symmetry of the crack and the infinite extent of the materials. In other words on the x boundaries, we assume the fields on both sides of the boundary oscillate in the same direction. To account for the even symmetry, we assign Neumann boundary conditions to these boundaries. In a similar manner, we assume the y boundaries are "sufficiently far" away from the sample and scanning area to not effect the overall measurements. Indeed, as the magnetic vector potential moves farther away from the sample and conducting sheet, $\mathbf{A}$ tends to zero. Therefore, on the y boundaries, we assign Dirichlet boundary conditions to indicate the boundary is "sufficiently far" away from the materials so that $\mathbf{A} \approx \mathbf{0}$. Therefore, the magnetic vector potential $\mathbf{A}$ is determined according to

$$\nabla \times \left(\frac{1}{\mu}\nabla \times \mathbf{A}\right) = \sigma(-i\omega\mathbf{A} - \nabla\phi) + i\omega\epsilon(-i\omega\mathbf{A} - \nabla\phi) \qquad \forall x, y \in \Omega.$$

and

$$I = \int_{cs} \mathbf{J} \cdot \mathbf{n} da = \int_{cs} (\sigma(-i\omega\mathbf{A} - \nabla\phi) + i\omega\epsilon(-i\omega\mathbf{A} - \nabla\phi)) \cdot \mathbf{n} da$$

with

$$\begin{array}{rcccl} \mathbf{A}(x,-35) & = & 0 & = & \mathbf{A}(x,35) \\ \nabla\mathbf{A}\cdot\mathbf{n}|_{(0,y)} & = & 0 & = & \nabla\mathbf{A}\cdot\mathbf{n}|_{(50,y)}. \end{array}$$

2 Computational Method

Our goal here is to characterize the geometry of a hidden i.e., subsurface, crack within a sample. To achieve this goal, we must develop fast and efficient forward computational methods to be used in the inverse problem possibly numerous times. To this end, we examine reduced order Karhunan-Loueve or Proper Orthogonal Decomposition (POD) techniques.

The POD technique is an attractive order reduction method, because basis elements are formed which span a data set consisting of experimental or numerical simulations in an "optimal" way. Since the POD basis is formed such that each basis captures important aspects of the data set, only a small

number of POD basis elements are needed in general to describe the solution [20]. Consequently, the POD method will enable us to formulate a fast forward algorithm which still describes the solution accurately with only a few basis elements.

2.1 The POD Method

We summarize the use of the POD method in the context of the inverse problem described above. For further details on the general POD method, we refer the reader to [1, 2, 3, 6, 13, 15, 16, 17, 18, 19, 20] and the extensive list of references contained therein. The first step in forming the POD basis is to collect "snapshots" or solutions across time, space or a varied parameter. In our case, we let $\mathbf{q}$ be the vector parameter characterizing physical properties of the damage, for example, the length, thickness, depth, center, etc. of the damage. For an ensemble of damages $\{\mathbf{q}_j\}_{j=1}^{N_s}$, we obtain corresponding solutions, $\{\mathbf{A}(\mathbf{q}_j)\}_{j=1}^{N_s}$, of (17), for magnetic vector potentials which we call our "snapshots". Alternatively, from the solution set $\{\mathbf{A}(\mathbf{q}_j)\}_{j=1}^{N_s}$, we can obtain the magnetic fluxes $\{\mathbf{B}(\mathbf{q}_j)\}_{j=1}^{N_s}$ and instead use these as our "snapshots" if we wish to treat magnetic fluxes as our basic state variable. However, for our explanation, we will consider snapshots on $\mathbf{A} = (0, 0, A_3)$ and hence our explanation will be for the scalar case. For the vector case, we would simply proceed componentwise [1, 6, 20]. Without loss of generality, we will denote the vector $\mathbf{A}$ by its scalar nonzero component A, i.e., the A_3 component of $\mathbf{A}$.

As explained in [20], we seek basis elements of the form

$$\Phi_i = \sum_{j=1}^{N_s} V_i(j) A(\mathbf{q}_j) \tag{20}$$

where the coefficients $V_i(j)$ are chosen such that each POD basis element Φ_i, $i = 1, 2, ..., N_s$, maximizes

$$\frac{1}{N_s} \sum_{j=1}^{N_s} |\langle A(\mathbf{q}_j), \Phi_i \rangle_{L^2(\Omega,\mathbb{C})}|^2$$

subject to $\langle \Phi_i, \Phi_i \rangle_{L^2(\Omega,\mathbb{C})} = ||\Phi_i||^2 = 1$. It is thus readily seen using standard arguments that the coefficients $V_i(j)$ are found by solving the eigenvalue problem

$$CV = \lambda V$$

where the covariant matrix C is given by

$$[C]_{ij} = \frac{1}{N_s}\langle A(\mathbf{q}_i), A(\mathbf{q}_j)\rangle_{L^2(\Omega,\mathbb{C})}.$$

Since the matrix C is a Hermitian positive semi-definite matrix, it possesses a complete set of orthogonal eigenvectors with corresponding real eigenvalues. We order the eigenvalues along with their corresponding eigenvectors such that the eigenvalues are in decreasing order,

$$\lambda_1 \geq \lambda_2 \geq ... \geq \lambda_{N_s} \geq 0.$$

We then normalize the eigenvectors corresponding to the rule

$$V_i \cdot V_j = \frac{\delta_{ij}}{N_s \lambda_j}.$$

Then the i^{th} POD basis element is defined by (20) where $V_i(j)$ represents the elements of the i^{th} eigenvector of C. It can also be shown that $\{\Phi_i\}_{i=1}^{N_s}$ are orthonormal in $L^2(\Omega, \mathbb{C})$ and $span\{\Phi_i\}_{i=1}^{N_s} = span\{A(\mathbf{q}_j)\}_{j=1}^{N_s}$. Indeed, given any $A(\mathbf{q}_j)$, we have

$$A(\mathbf{q}_j) = \sum_{k=1}^{N_s} \alpha_k(\mathbf{q}_j)\Phi_k$$

where

$$\alpha_k(\mathbf{q}_j) = \langle A(\mathbf{q}_j), \Phi_k\rangle_{L^2(\Omega,\mathbb{C})}.$$

To determine the reduced number, N, of POD basis elements required to accurately portray the ensemble of "snapshots" $\{A(\mathbf{q}_j)\}_{j=1}^{N_s}$, we compute

$$\sum_{j=1}^{N} \lambda_j / \sum_{i=j}^{N_s} \lambda_j$$

which represents the percentage of "energy" in $span\{A(\mathbf{q}_j)\}_{j=1}^{N_s}$ that is captured in $span\{\Phi_j)\}_{j=1}^{N}$. The reduced basis consists of only the first N elements Φ_i where N is chosen according to the percentage "energy" desired. From these N POD basis elements, we obtain the approximation $A^N(\mathbf{q}_j)$ for $A(\mathbf{q}_j)$ such that

$$A(\mathbf{q}_j) \approx A^N(\mathbf{q}_j) \equiv \sum_{k=1}^{N} \alpha_k(\mathbf{q}_j)\Phi_k.$$

To approximate $A^N(\mathbf{q})$ where $\mathbf{q}$ is a given parameter *not* in the set $\{\mathbf{q}_j\}_{j=1}^{N_s}$, we extend the approximation formula to obtain

$$A^N(\mathbf{q}) = \sum_{k=1}^{N} \alpha_k(\mathbf{q})\Phi_k$$

where

$$\alpha_k(\mathbf{q}) \equiv \alpha_k(\mathbf{q}_j) + [\alpha_k(\mathbf{q}_{j+1}) - \alpha_k(\mathbf{q}_j)]\frac{(\mathbf{q}-\mathbf{q}_j)\cdot(\mathbf{q}_{j+1}-\mathbf{q}_j)}{|\mathbf{q}_{j+1}-\mathbf{q}_j|^2}$$

with $\mathbf{q}_j$ and $\mathbf{q}_{j+1}$ "nearest" neighbors to $\mathbf{q}$.

Once we have the solution $A^N(\mathbf{q})$, we can recapture the explicit time dependence by referring to the formula (1) in Section 1.2 given by

$$\overline{\mathbf{A}}(x,y,t) = Re(\mathbf{A}(x,y)e^{i\omega t}).$$

2.2 Inverse Problem

Using the methodology presented in the previous section for calculating the magnetic vector potential A given specific crack parameters, we shall try to identify these crack parameters. In identifying the geometry of a crack, we would like to estimate the length, thickness, center and depth of a crack within a sample. To determine the feasibility of this task and to illustrate the use of the reduced model methodology, we first try to estimate a single parameter, say length or thickness, while assuming the values of the other parameters are known quantities. If this can be successfully done, further efforts at estimating two or more parameters can be pursued.

2.2.1 Least Squares Criterion

In our trial runs, we assume we have access to various types of data, such as the $\mathbf{A}$ field or the $\mathbf{B}$ field, in various points of space, which we call the set Ψ. We compare and contrast the accuracy to which we can estimate the given parameter or parameters based upon the field i.e., $\mathbf{A}$ or $\mathbf{B}$, to which we have access as well as what an appropriate choice of the points in Ψ should be.

For example, we assume the unknown parameter set contains only values of the parameter lengths l. That is, we want to estimate only the length of the crack assuming the thickness, center, and depth are fixed quantities. Given an arbitrary length l, we can generate a solution $A^N(l)$, the computed solution A^N as described in Section 2.1. We can compare the computed solution to the experimental or simulated data $\hat{A}(l^*)$ for the exact parameter

value l^*. For the examples presented here, we choose the parameter values for equations (17) and (19) given in Table 1. However, for the system values

Table 1: Parameters Used in Equation (17) for Computational Results

Parameter	Value
ω	$2\pi f$
f	$60Hz$
σ_{al}	$3.72 \times 10^7 \frac{S}{m}$
σ_{cu}	$5.80 \times 10^7 \frac{S}{m}$
σ_{air}	$0\frac{S}{m}$
I	$1A$

given, the order of magnitude of A is $10^{-8}\frac{Wb}{m}$; therefore it is desirable to scale both the data and the computed solution to achieve a more accurate estimation. If the data is below the desired tolerance of the optimizaton routine used, the matlab based routine *nelder* in our case, the converged estimated value will be the initial guess. Therefore, in this case, we want to minimize the least squares criterion

$$J(l) = \sum_{i=1}^{n}\sum_{j=1}^{m} |10^8 A^N(x_i, y_j, l) - 10^8 \hat{A}(x_i, j_j, l^*)| \tag{21}$$

over the set of all possible length values where $(x_i, y_j), i = 1, ..., n; j = 1, ..., m$ are points in the set Ψ. The set Ψ, in our trial runs, varies from a set of points uniformly discretizing all of Ω to simply one line of sample points above the conducting sheet or one line below the sample with a grid spacing of $0.5mm$ in both the x and y direction. If we assume we have access to the values of $\hat{A}$ in all of Ω, in other words values in the conducting sheet and the sample as well the air above the conducting sheet, below the sample, and in between the sample and conducting sheet, the set Ψ is thus given by

$$\Psi = \{(x_i, y_j) \in \Omega | x_i = (0.5i)mm, i = 0, ..., 100; y_j = (0.5j - 35)mm, j = 0, ..., 140\}.$$

If instead we assume we only have access to values on a line $1mm$ above the conducting sheet, the set Ψ is given by

$$\Psi = \{(x_i, y) \in \Omega | x_i = (0.5i)mm, i = 0, ..., 100; y = 2mm\}$$

(the top of the conducting sheet is at $y = 1mm$). We can describe Ψ similarly for other choices of data sets.

In most experimental settings, we do not have access to measurements of the magnetic vector potential $\mathbf{A}$, but instead to those of the magnetic field $\mathbf{B}$. In this case, we compute $\mathbf{A}^N(l)$ for a given l in the manner described in Section 2.1. To find the computed magnetic field $\mathbf{B}^N(l)$, we simply use the definition

$$\mathbf{B}^N(l) = \nabla \times \mathbf{A}^N(l).$$

In general, it is not necessary to use the entire $\mathbf{B}$ field, but instead we can use only one component of the $\mathbf{B}$ field, either the x component, B_1, or the y component, B_2. If we are using the x component of $\mathbf{B}$, our least squares criterion would be

$$J(l) = \sum_{i=1}^{n} \sum_{j=1}^{m} |10^8 B_1^N(x_i, y_j, l) - 10^8 \hat{B}_1(x_i, j_j, l^*)|; \tag{22}$$

whereas, if we use the y component of the $\mathbf{B}$ field, the criterion would be

$$J(l) = \sum_{i=1}^{n} \sum_{j=1}^{m} |10^8 B_2^N(x_i, y_j, l) - 10^8 \hat{B}_2(x_i, j_j, l^*)| \tag{23}$$

where $(x_i, y_j) \in \Psi$. We minimize the three criteria, (21), (22), and (23), along various sets Ψ and determine which criterion allows us to most accurately determine the unknown parameter l while allowing for the limitations of the given set Ψ. Similarly, we can estimate other unknown parameters in a similar manner where we replace l by $\mathbf{q}$ in the above equations where $\mathbf{q}$ represents the entire set of unknown parameters.

2.2.2 Noise Generator

In the samples provided, simulated data was used to represent experimental data $\hat{A}$, $\hat{B}_1$, or $\hat{B}_2$, depending upon the specific trial run. To obtain the simulated data, we specified the parameters $\mathbf{q}^*$ for a crack and generated the solution based upon these exact parameters using the commercial software Ansoft Maxwell 2D Field Simulator. Again, the goal is to recapture these parameters by minimizing one of the cost functions given above. However, when using actual experimental data, we sometimes have random error in the measurements taken. To simulate this random error, we add random noise to the simulated data to test our methodology in the presence of noise.

To generate the noise, we use the Matlab function *randn* which generates a normally distributed set of random numbers with mean 0 and variance

1. A normally distributed set of random numbers has a 65% certainty of being within 1 standard deviation, 95% certainty of being within 2 standard deviations and 99.7% certainty of being within 3 standard deviations of the mean. In other words, there is a 65% chance the Matlab function *randn* will return a number in the interval $(-1, 1)$, 95% chance of returning a number in the interval $(-2, 2)$ and a 99.7% chance of producing a number in the interval $(-3, 3)$. Therefore, we can control the amount of noise in the simulated data by scaling the certainty intervals.

For example, assume we have generated the solution $\hat{A}(\mathbf{q}^*)$ given exact parameters $\mathbf{q}^*$. Furthermore, we assume we desire to be 95% certain that the noise generated is within 1% of the actual data $\hat{A}(\mathbf{q}^*)$. For 95% certainty of 1% noise, we want to scale the interval $(-2, 2)$ to be $(-0.01, 0.01)$. Therefore, letting

$$\epsilon_1 = 0.005 * randn,$$

the data with 95% certainty of having 1% relative noise, $\tilde{A}$, is given by

$$\tilde{A}(\mathbf{q}^*) = \hat{A}(\mathbf{q}^*)(1 + \epsilon_1).$$

Similarly, if we instead want to be 99.7% certain of noise within 1% of the simulated data, we scale the interval $(-3, 3)$ to the interval $(-0.01, 0.01)$ or let

$$\epsilon_2 = 0.0033 * randn.$$

Again, the data with 99.7% certainty of having 1% relative noise, $\tilde{A}$, is given by

$$\tilde{A}(\mathbf{q}^*) = \hat{A}(\mathbf{q}^*)(1 + \epsilon_2).$$

In the trials we performed, we simulated corrupted experimental data by generating noise at a 1% relative noise level with both 95% certainty and 99.7% certainty as discussed above as well as noise at a 5% and 10% relative noise level with both 95% certainty and 99.7% certainty.

2.3 Results with Test Examples

In determining the geometry of the crack in our simulations, we focus first on determining the length of the damage and then separately the thickness of the damage. Various trials are performed in each case for which the specific values can be found in the Appendices. A summary of the results will be given in this section.

2.3.1 Determining the Length of the Damage

The first step in determining the length of the damage is to generate an ensemble of damages with various crack lengths $\{l_j\}_{j=1}^{N_s}$ to be used in forming the POD basis. In generating the damages for the examples reported on here, we used crack lengths varying from $0mm$ to $4mm$ in increments of $0.2mm$ while keeping the thickness of the crack fixed at $2mm$ ($N_s = 21$). We then used the commercial software Ansoft Maxwell 2D Field Simulator to generate the snapshots $\{A(l_j)\}_{j=1}^{21}$. Based upon the calculations discussed in Section 2.1, 99.99% of the energy of the system was captured with a single basis element. Table 2 gives the amount of energy captured when using N basis elements, up to 10 basis elements.

Table 2: Energy Captured with N Basis Elements using Snapshots of A on Length

N	Energy Captured
1	0.99999469355655
2	0.99999998707290
3	0.99999999918539
4	0.99999999978293
5	0.99999999987493
6	0.99999999990451
7	0.99999999992129
8	0.99999999993439
9	0.99999999994409
10	0.99999999995308

To test the inverse methodology, we first try to identify the length of the damage, $l^* = 1.3mm$, by using the criterion given in equation (21). We ran the inverse problem using $1, 2, 3, 4$ and 5 reduced POD basis elements with data containing no noise over the entire discretized region Ω. There was no noticeable difference between using 4 and 5 basis elements; hence we chose to use 4 POD basis elements in our solution approximation.

Based upon the results (see Appendix A.1), we can conclude that under the assumption that we have access to the magnetic vector potential A in all of Ω, we did a good job of estimating the crack length even when the data contained 5% relative noise. In actuality, however, we only have access to data in the regions of air above the conducting sheet or below the sample. Therefore, the inverse problem was next carried out using "data" in just

these regions. The results (Appendices A.2 and A.7) illustrate that we still do a reasonable job estimating the crack length. Although technically it is possible to have access to data in the entire region of air, typically data is only taken on only one or two lines above the conducting sheet or below the sample. As a result of running the inverse problem on just a few lines above the conducting sheet or below the sample, the inverse problem did not seem to be efficient, especially for data containing noise at the 5% level. The results (Appendices A.3 - A.6, A.8 - A.11) indicate that if there is a considerable amount of noise (5% noise level in our case), it is not feasible to accurately estimate the crack length using the magnetic vector potential A. Even with a small amount of noise in the data, the results are not as accurate as we would like.

As we have already noted, in experimental situations we do not have access to the magnetic vector potential. Instead, we only have access to the magnetic flux density or the magnetic field. As a result, we repeated the computational tests as reported in Appendix A with the exception of using the criteria given by expressions (22) and (23). Using B_1 data or the criterion (22), the results were no better than when we used the magnetic vector potential (see Appendix B). On the other hand, when we used B_2 data (Appendix C), criterion (23), the inverse problem produced remarkably accurate results; estimated lengths were accurate to an order of 10^{-3}. However, the most notable observation in using B_2 data is the low variation in results even at the 5% and 10% relative noise level. Based upon these results, we could quite accurately estimate a given length of a crack even if the data contained a considerable amount of noise. Therefore, we concluded that even when scanning along a single line, when using the y component of the magnetic flux density, we can accurately recapture the length of a crack within a sample. Scanning along multiple lines or over the whole region only provided marginal improvements in the estimated length; the improvements are not sufficiently substantial to warrant the extra time or money required to obtain the extra data.

The results above were produced by taking snapshots of the magnetic vector potential. We also took snapshots (with which we formed POD basis elements) on the y component of the magnetic flux density, B_2, and performed the analysis again using the criterion (23) (see Appendix D). Although there was a quite notable difference in the energy captured in N basis elements, see Table 3, the inverse problem still showed the same consistency and accuracy as seen previously. One comparison we can make between using POD elements resulting from snapshots of A versus snapshots of B_2 in the inverse problem is that when using the snapshots on A, the es-

timated length was normally an overestimate. Conversely, using the POD elements resulting from snapshots on B_2 usually yielded an underestimate of the length. Despite this fact, there seems to be no other apparent difference in using the snapshots on A to generate the basis elements as opposed to using the snapshots on B_2 to generate the basis elements, as long as one uses the criterion (23) in the inverse problem calculations.

Table 3: Energy Captured with N Basis Elements using Snapshots of B_2 on Length

N	Energy Captured
1	0.95752844126957
2	0.98938760682215
3	0.99515414870549
4	0.99680555604825
5	0.99749219883487
6	0.99789119249012
7	0.99822617546932
8	0.99853187498393
9	0.99871258779223
10	0.99888757131260

2.3.2 Determining the Thickness or Height of the Damage

Proceeding as we did in estimating the length of a damage, we generated an ensemble of crack thicknesses (heights) ranging from $0mm$ to $4mm$ in increments of $2mm$, $\{h_j\}_{j=1}^{21}$ with associated solutions $\{A(h_j)\}_{j=1}^{21}$. Similar to taking snapshots on the length of a damage, 99.99% of the energy was captured in a single basis element, see Table 4.

Based upon the results on characterizing the length of the damage, we only considered snapshots of the magnetic vector potential and B_2 data in the inverse problem. However, unlike when estimating the length of the crack, even though 99% of the energy is captured in a single basis element even when we snapshot on B_2, see Table 5, more basis elements (at least 8) were required in the inverse problem to estimate the thickness of the crack with an accuracy of order 10^{-3} when no noise was added using just one line above the conducting sheet. Therefore, we used 9 POD basis elements. Although more basis elements were used, the total time required to recapture the thickness of the crack was still only 8 seconds. Furthermore, the results

Table 4: Energy Captured with N Basis Elements using Snapshots of A on Thickness

N	Energy Captured
1	0.99999446453503
2	0.99999999666469
3	0.9999999993584
4	0.99999999961479
5	0.99999999972048
6	0.99999999980054
7	0.99999999984470
8	0.99999999987779
9	0.99999999990521
10	0.99999999992316

(see Appendix E) when using 9 POD basis elements were still accurate even in the presence of 10% noise. Thus, similar to estimating the length of a crack, we can also recapture the thickness of a crack quite accurately and efficiently.

Table 5: Energy Captured with N Basis Elements using Snapshots of B_2 on Thickness

N	Energy Captured
1	0.99488023435913
2	0.99728234129540
3	0.99799825670140
4	0.99836722535293
5	0.99870058186819
6	0.99896958827131
7	0.99911070207772
8	0.99923141472559
9	0.99934263323537
10	0.99944776176825

3 Conclusion

In this paper, we began by developing a two-dimensional test problem to be used in locating and characterizing the geometry of a hidden damage within a sample of material. This two-dimensional problem was argued to be a reasonable approximation to a typical three-dimensional problem under certain assumptions. We then formulated the forward problem describing the behavior of the magnetic vector potential in this test problem and discussed computational methods to be used in solving the forward problem. In order to quickly and efficiently obtain results in the inverse problem, the computational methods for the forward problem must be fast and accurate. Therefore, we chose to use the reduced order POD technique in the forward problem, allowing us to use less than 10 basis elements in each of the examples tested to date. Consequently, we were able to provide a fast forward algorithm. Moreover, the POD basis elements were formed so that we captured at least 99% of the energy in these few basis elements, making the foward algorithm accurate as well as fast.

We then explained the implementation of the inverse problem and results. While the methods did not seem to be robust when using A data or B_1 data in the inverse algorithm, the methods were robust, even in the presence of 10% relative noise, when using B_2 data regardless of whether we snapshot on the magnetic vector potential or the magnetic flux density. Furthermore, performing multi-line scans or using full region data improve results only marginally over a single line scan and hence do not warrant the extra effort and time in collecting more extensive data sets. Moreover, if one were to use a software package such as Ansoft's Maxwell 2D Field Simulator to calculate the forward problem each time required in the inverse problem, it would take approximately 5-10 minutes for a *single* forward run and hence any inverse algorithm based on this forward solver would require hours of time for the optimization problem. In using the reduced order POD methodology for the forward problem, the *entire* inverse problem takes approximately 8 seconds, less than $\frac{1}{30}$ the time required for a single forward run using Ansoft. As a forward algorithm is called numerous times, this is a substantial reduction in time required. Therefore, using data collected on a single line above the conducting sheet or below the sample, we are able to estimate the length or thickness of a damage in a small amount of time.

The results summarized in this note suggest that use of the POD based approximation methods in electromagnetic eddy current technique inverse problems for damage is a viable approach. We are therefore continuing our efforts with damages requiring more than one-dimensional parameterization.

We are also exploring use of these techniques in geometries requiring 3D formulations.

Acknowledgements

This research was supported in part (MLJ) by the NASA Langley Graduate Researcher's Program under grant NGT-1-52196, in part (MLJ) by the Air Force Office of Scientific Research under grant AFSOR F49620, and in part (MLJ and HTB) under grant AFSOR F49620-91-1-0180. Part of the research was carried out while the first two authors were visitors at the Institute for Computer Applications in Science and Engineering (ICASE), NASA Langley Research Center, Hampton, Va, which is operated under contract NAS1-97046.

References

[1] Banks, H.T., del Rosario, R.C. and Smith, R.C., *Reduced Order Model Feedback Control Design: Numerical Implementation in a Thin Shell Model*, Tech. Rep. CRSC-TR98-27, July, 1998; IEEE Trans. Auto. Control, to appear.

[2] Berkooz, G. *Observations on the Proper Orthogonal Decomposition*, Studies in Turbulence, Springer-Verlag, New York (1992), pp. 229-247.

[3] Berkooz, G., Holmes, P., and Lumley, J.L. *The Proper Orthogonal Decomposition in the Analysis of Turbulent Flows*, Annual Review of Fluid Mechanics, Vol. 25 (1993), N5:539-575.

[4] Cheng, D.K. Field and Wave Electromagnetics, Addison-Wesley, Reading, Mass., 1989.

[5] Cochran, A., Dondaldson, G.B., Carr, C., McKirdy, D.McA., Walker, M.E., Klein, U., Kuznik, J. and McNab, A. *Advances in the Theory and Practice of SQUID NDE*, Review in Progress in QNDE, Vol. 15 (1996), 1151-1158.

[6] del Rosario R.C., *Computational Methods for Feedback Control in Structural Systems*, PhD thesis, N.C. State University, pp. 48-51, 1998.

[7] Donaldson, G.B. and McKirdy, D.McA. *The Use of SQUIDs for Nondestructive Evaluation*, SQUID Sensors: Fundamentals, Fabrication and Application, 1996, 599-628.

[8] Fitzpatrick, G.L., Thorne, D.K., Skaugset, R.L., Shih, E.Y.C. and Shih, W.C.L. *Magneto-Optic/Eddy Current Imaging of Aging Aircraft: A New NDI Technique*, Materials Evaluation, 1993, 1402-1407.

[9] Guettinger, T.W., Grotz, K. and Wezel, H. *Eddy Current Imaging*, Materials Evaluation, April 1993, 444-451.

[10] Haywood, N.C. and Bowler, J.R. *Eddy-Current Imaging of Buried Cracks by Inverting Field Data*, IEEE Trans. On Magnetics, Vol. 28, Number 2, 1336-1339.

[11] Jacson, J.D. Classical Electrodynamics, 2nd edition, John Wiley and Sons, New York, 1975.

[12] Jenks, W.G. and Wikswo Jr., J.P. *Review Article: SQUIDs for Nondestructive Evaluation*, Journal of Physics D: Applied Physics, Volume 30 (1997), 293-323.

[13] Karhunen, K. *Zur Spektral Theorie Stochasticher Prozesse*, Ann. Acad. Sci. Fennicae, Ser. A1 Math Phys., Vol. 37 (1946).

[14] Kepler, G.M., Tran, H.T. and Banks, H.T., *Reduced Order Model Compensator Control of Species Transport in a CVD Reactor*, Tech. Rep. CRSC-TR99-15, April, 1999; Optimal Control: Applications and Methods, submitted.

[15] Kirby, M. and Sirovich, L. *Application of the Karhunen-Loeve Procedure for the Characterization of Human Faces*, IEEE Transactions on Pattern Analysis and Machine Intelligence, Vol. 12 (1990), N1:103-108.

[16] Kirby, M., Boris, J.P., and Sirovich, L. *A Proper Orthogonal Decomposition of a Simulated Supersonic Shear Layer*, International Journal for Numerical Methods in Fluids, Vol. 10 (1990), pp.411-428.

[17] Loeve, M. *Functions aleatoire de second ordre*, Compte rend. Acad. Sci. (Paris), 1945, p.220.

[18] Lumley, J.L. *The Structure of Inhomogeneous Turbulent Flows*, Atmospheric Turbulence and Radio Wave Propagation, Moscow: Nauka (1967), pp.166-178.

[19] Lumley, J.L. *Stochastic Tools in Turbulence*, Academic Press, New York (1970).

[20] Ly, H.V. and Tran H.T., *Proper Orthogonal Decomposition for Flow Calculations and Optimal Control in a horizontal CVD Reactor*, Tech. Rep. CRSC-TR98-13, March, 1998; Quart. Applied Math, to appear.

[21] Ma, Y.P. and Wikswo, Jr., J.P. *Imaging Subsurface Defects Using a SQUID Magnetometer*, Review of Progress in QNDE, Volume 12A, (1993), 1137-1143.

[22] Maxwell 2D Field Simulator Version 6.5.04 - Technical Notes, 1997 Ansoft Corporation, 14-16.

[23] McKirdy, D. McA., Cochran, A., Donaldson, G.B. and McNab, A. *Forward and Inverse Processing in Electromagnetic NDE Using SQUIDs*, Review of Progress in QNDE, 1996, 347-354.

[24] Thorne D.K., Fitzpatrick, G.L., Shih, E.Y.C. and Shih, W.C.L., *Aircraft Inspection with the Magneto-Optic/Eddy Current Imager - A New Technology*, presented at the ATA NDT Forum, Long Beach, CA, Sept. 10-12, 1991.

[25] Wienstock, H. *A Review of SQUID Magnetometry Applied to Nondestructive Evaluation*, IEEE Transactions on Magnetics, Volume 27, Number 2, (1991), 3131-3236.

[26] Wincheski B., Fulton, J., Nath, S., Namking, M. and Simpson, J. *Self-Nulling Eddy Current Probe for Surface amd Subsurface Flaw Detection*, Materials Evaluation, Vol. 52, Number 1, (Jan. 1994), 22-26.

[27] Wincheski B., Fulton, J., Nath, S. and Namkung, M. *Analysis of Eddy Current Distribution and Resulting Flaw Detection Mechanism for Self-Nulling Probe*, Review of Progress in Quantitative NDE, Vol. 14A, (1995), 291-298.

Appendices

A Results Varying the Length using A for the POD elements and A in the Inverse Problem

A.1 All of Ω

A.1.1 No noise: 1.2999

A.1.2 1% noise

1% noise (95%)			1% noise (99.7%)	
Trial	Est. l		Trial	Est l
1	1.3164		1	1.3023
2	1.3140		2	1.3140
3	1.3091		3	1.2943
4	1.3160		4	1.3021
5	1.30007		5	1.2898
6	1.3026		6	1.2932
7	1.3127		7	1.3112
8	1.2829		8	1.2979
9	1.2876		9	1.2916
10	1.3044		10	1.3041
Mean 1.3046	Median 1.3067		Mean 1.3000	Median 1.3000
St. Dev. 0.0117	Var $0.1360 * 10^{-3}$		St. Dev. 0.0082	Var. $0.6716 * 10^{-4}$

A.1.3 5% noise

5% noise (95%)			5% noise (99.7%)	
Trial	Est. l		Trial	Est l
1	1.3474		1	1.2931
2	1.3104		2	1.3428
3	1.2729		3	1.2612
4	1.2656		4	1.3333
5	1.3369		5	1.2515
6	1.2769		6	1.3818
7	1.1103		7	1.3596
8	1.2874		8	1.2767
9	1.2635		9	1.3481
10	1.3159		10	1.3114
Mean 1.2787	Median 1.2821		Mean 1.3160	Median 1.3224
St. Dev. 0.0661	Var 0.0044		St. Dev. 0.0441	Var. 0.0019

A.2 Air above Conducting Sheet

A.2.1 No noise: 1.2997

A.2.2 1% noise

1% noise (95%)			1% noise (99.7%)	
Trial	Est. l		Trial	Est l
1	1.3425		1	1.2129
2	1.3177		2	1.3241
3	1.2542		3	1.3352
4	1.2837		4	1.3020
5	1.3171		5	1.2832
6	1.2633		6	1.3098
7	1.2488		7	1.2744
8	1.3755		8	1.2953
9	1.2717		9	1.2661
10	1.3580		10	1.2775
Mean	Median		Mean	Median
1.3033	1.3004		1.2880	1.2892
St. Dev.	Var		St. Dev.	Var.
0.0454	0.0021		0.0345	0.0012

A.2.3 5% noise

5% noise (95%)			5% noise (99.7%)	
Trial	Est. l		Trial	Est l
1	1.5417		1	1.3383
2	1.7327		2	1.2235
3	1.4729		3	1.2000
4	1.3760		4	1.2227
5	1.6875		5	1.1396
6	1.5942		6	1.1630
7	0.7461		7	1.2158
8	1.3169		8	1.2349
9	1.0796		9	1.2936
10	1.2246		10	1.4727
Mean	Median		Mean	Median
1.3772	1.4244		1.2504	1.2231
St. Dev.	Var		St. Dev.	Var.
0.3018	0.0911		0.0968	0.0094

A.3 1 line $1mm$ above Conducting Sheet

A.3.1 No noise: 1.3008

A.3.2 1% noise

1% noise (95%)			1% noise (99.7%)	
Trial	Est. l		Trial	Est l
1	1.5117		1	1.2520
2	1.4375		2	1.0215
3	0.9785		3	1.3027
4	1.1621		4	1.0781
5	1.1592		5	1.4512
6	1.0400		6	1.4365
7	0.6377		7	1.4219
8	1.5977		8	1.4072
9	1.4189		9	1.0796
10	0.7861		10	1.3535
Mean	Median		Mean	Median
1.1729	1.1606		1.2804	1.3281
St. Dev.	Var		St. Dev.	Var.
0.3193	0.1019		0.1648	0.0272

A.3.3 5% noise

5% noise (95%)			5% noise (99.7%)	
Trial	Est. l		Trial	Est l
1	1.8438		1	0.8706
2	2.5371		2	3.1279
3	2.2451		3	0.8486
4	2.2910		4	2.4487
5	0.1699		5	0.9888
6	0.0820		6	0.2402
7	0.2148		7	1.8872
8	0.8770		8	1.0327
9	0.0000		9	1.5786
10	3.8301		10	0.8496
Mean	Median		Mean	Median
1.4091	1.3604		1.3873	1.0107
St. Dev.	Var		St. Dev.	Var.
1.3246	1.7545		0.8749	0.7655

A.4 2 lines $1mm$ & $1.5mm$ above Conducting Sheet

A.4.1 No noise: 1.3008

A.4.2 1% noise

1% noise (95%)			1% noise (99.7%)	
Trial	Est. l		Trial	Est l
1	1.2979		1	1.4248
2	1.0068		2	1.5068
3	1.1875		3	1.5845
4	1.5322		4	1.2759
5	1.5078		5	1.3535
6	1.2227		6	1.0981
7	1.5635		7	1.4292
8	1.1572		8	1.5376
9	1.1221		9	1.4912
10	1.0190		10	1.3921
Mean	Median		Mean	Median
1.2617	1.2051		1.4094	1.4270
St. Dev.	Var		St. Dev.	Var.
0.2075	0.0430		0.1422	0.0202

A.4.3 5% noise

5% noise (95%)			5% noise (99.7%)	
Trial	Est. l		Trial	Est l
1	0.0000		1	0.1797
2	2.1362		2	0.3955
3	2.4600		3	1.7627
4	1.0371		4	1.0664
5	0.1758		5	3.0376
6	0.1680		6	0.8433
7	2.0000		7	1.4243
8	2.0488		8	2.2070
9	1.8364		9	1.5337
10	0.0000		10	0.3496
Mean	Median		Mean	Median
1.1862	1.4368		1.2800	1.2454
St. Dev.	Var		St. Dev.	Var.
1.0137	1.0276		0.9044	0.8180

A.5 2 lines $1mm$ & $2mm$ above Conducting Sheet

A.5.1 No noise: 1.3008

A.5.2 1% noise

1% noise (95%)			1% noise (99.7%)	
Trial	Est. l		Trial	Est l
1	1.6216		1	1.3755
2	1.2178		2	1.3252
3	1.2305		3	1.2856
4	1.3145		4	1.1709
5	1.3877		5	1.2666
6	1.1328		6	1.4526
7	1.2178		7	1.2051
8	0.9541		8	1.3071
9	1.5146		9	1.1025
10	1.2446		10	1.3955
Mean 1.2836	Median 1.2375		Mean 1.2887	Median 1.2964
St. Dev. 0.1897	Var 0.0360		St. Dev. 0.1072	Var. 0.0115

A.5.3 5% noise

5% noise (95%)			5% noise (99.7%)	
Trial	Est. l		Trial	Est l
1	0.2710		1	1.7476
2	0.0000		2	1.4482
3	2.3340		3	0.5010
4	0.8428		4	1.4795
5	1.3818		5	0.9219
6	0.7466		6	1.8154
7	1.4355		7	0.1602
8	1.3960		8	0.3975
9	1.0332		9	0.1470
10	2.2305		10	2.0205
Mean 1.1671	Median 1.2075		Mean 1.0639	Median 1.1851
St. Dev. 0.7548	Var 0.5698		St. Dev. 0.7231	Var. 0.5229

A.6 3 lines $1mm$, $1.5mm$ & $2mm$ above Conducting Sheet

A.6.1 No noise: 1.3008

A.6.2 1% noise

1% noise (95%)			1% noise (99.7%)	
Trial	Est. l		Trial	Est l
1	1.2148		1	1.3882
2	1.1426		2	1.2534
3	1.2510		3	1.3403
4	1.4546		4	1.3447
5	1.5117		5	1.2095
6	1.2319		6	1.3442
7	1.1025		7	1.2661
8	1.4028		8	1.5513
9	1.4668		9	1.3965
10	1.3750		10	1.4624
Mean	Median		Mean	Median
1.3154	1.3130		1.3557	1.3445
St. Dev.	Var		St. Dev.	Var.
0.1447	0.0209		0.1015	0.0103

A.6.3 5% noise

5% noise (95%)			5% noise (99.7%)	
Trial	Est. l		Trial	Est l
1	1.9707		1	1.3916
2	0.9438		2	1.7456
3	3.2266		3	2.2070
4	1.1763		4	1.8628
5	2.2183		5	1.1856
6	0.0000		6	1.1016
7	1.7520		7	1.7388
8	1.8276		8	2.6826
9	1.5508		9	1.2510
10	0.0000		10	1.3896
Mean	Median		Mean	Median
1.4666	1.6514		1.6557	1.5652
St. Dev.	Var		St. Dev.	Var.
0.9885	0.9772		0.4998	0.2498

A.7 Air below Sample

A.7.1 No noise: 1.2988

A.7.2 1% noise

1% noise (95%)			1% noise (99.7%)	
Trial	Est. l		Trial	Est l
1	1.2954		1	1.2881
2	1.2969		2	1.3003
3	1.2729		3	1.2881
4	1.2932		4	1.2998
5	1.3010		5	1.3027
6	1.2710		6	1.3199
7	1.2842		7	1.3228
8	1.2998		8	1.3142
9	1.3225		9	1.3105
10	1.3188		10	1.2783
Mean 1.2956	Median 1.2961		Mean 1.3025	Median 1.3015
St. Dev. 0.0169	Var $0.2853 * 10^{-3}$		St. Dev. 0.0146	Var. $0.2138 * 10^{-3}$

A.7.3 5% noise

5% noise (95%)			5% noise (99.7%)	
Trial	Est. l		Trial	Est l
1	1.0972		1	1.3926
2	1.4709		2	1.2100
3	1.3215		3	1.1553
4	1.1084		4	1.3296
5	1.4141		5	1.3301
6	1.1543		6	1.3179
7	1.2007		7	1.3762
8	1.3455		8	1.2281
9	1.3677		9	1.3574
10	1.3105		10	1.4438
Mean 1.2791	Median 1.3160		Mean 1.3141	Median 1.3298
St. Dev. 0.1308	Var 0.0171		St. Dev. 0.0899	Var. 0.0081

A.8 1 line $1mm$ below Sample

A.8.1 No noise: 1.3008

A.8.2 1% noise

1% noise (95%)			1% noise (99.7%)	
Trial	Est. l		Trial	Est l
1	1.2070		1	1.3398
2	1.2266		2	1.2461
3	1.2803		3	1.3291
4	1.2402		4	1.3164
5	1.1992		5	1.2979
6	1.2930		6	1.2217
7	1.3672		7	1.3770
8	1.3154		8	1.3076
9	1.3242		9	1.2480
10	1.1396		10	1.2939
Mean	Median		Mean	Median
1.2593	1.2603		1.2978	1.3027
St. Dev.	Var		St. Dev.	Var.
0.0689	0.0047		0.0476	0.0023

A.8.3 5% noise

5% noise (95%)			5% noise (99.7%)	
Trial	Est. l		Trial	Est l
1	0.8916		1	1.4160
2	1.2363		2	0.9141
3	1.0332		3	1.4346
4	1.2539		4	1.7129
5	1.3506		5	1.5127
6	1.5488		6	1.2480
7	0.5635		7	1.2979
8	1.3018		8	1.0947
9	2.1152		9	1.5430
10	1.2422		10	1.2773
Mean	Median		Mean	Median
1.2537	1.2480		1.3451	1.3569
St. Dev.	Var		St. Dev.	Var.
0.4079	0.1664		0.2310	0.0539

A.9 2 lines $1mm$ & $1.5mm$ below Sample

A.9.1 No noise: 1.3008

A.9.2 1% noise

1% noise (95%)			1% noise (99.7%)	
Trial	Est. l		Trial	Est l
1	1.2798		1	1.2559
2	1.2812		2	1.3301
3	1.2974		3	1.3545
4	1.3247		4	1.2695
5	1.3945		5	1.2802
6	1.2109		6	1.3203
7	1.3301		7	1.3145
8	1.2725		8	1.3125
9	1.3242		9	1.3374
10	1.2500		10	1.2197
Mean	Median		Mean	Median
1.2965	1.2893		1.2995	1.3135
St. Dev.	Var		St. Dev.	Var.
0.0504	0.0025		0.0418	0.0017

A.9.3 5% noise

5% noise (95%)			5% noise (99.7%)	
Trial	Est. l		Trial	Est l
1	1.3135		1	1.0977
2	1.4316		2	1.2305
3	1.3662		3	1.3076
4	0.8086		4	1.4883
5	1.4004		5	1.4893
6	1.7168		6	1.6211
7	0.9863		7	1.3965
8	1.3965		8	1.0483
9	1.4004		9	1.1406
10	1.2900		10	1.4414
Mean	Median		Mean	Median
1.3110	1.3813		1.3261	1.3521
St. Dev.	Var		St. Dev.	Var.
0.2503	0.0626		0.1919	0.0368

A.10 2 lines $1mm$ & $2mm$ below Sample

A.10.1 No noise: 1.3008

A.10.2 1% noise

1% noise (95%)			1% noise (99.7%)	
Trial	Est. l		Trial	Est l
1	1.3232		1	1.8330
2	1.2451		2	1.3125
3	1.2539		3	1.2563
4	1.3975		4	1.3213
5	1.3135		5	1.3047
6	1.4102		6	1.3330
7	1.3740		7	1.2769
8	1.2461		8	1.3130
9	1.2402		9	1.2920
10	1.2808		10	1.3320
Mean 1.3084	Median 1.2971		Mean 1.3075	Median 1.3127
St. Dev. 0.0659	Var 0.0043		St. Dev. 0.0257	Var. $0.6614 * 10^{-3}$

A.10.3 5% noise

5% noise (95%)			5% noise (99.7%)	
Trial	Est. l		Trial	Est l
1	1.3506		1	1.1978
2	0.8071		2	1.0562
3	7.1978		3	1.4238
4	1.4679		4	0.9912
5	1.1035		5	1.4028
6	0.8970		6	1.4590
7	1.0308		7	1.3076
8	1.6934		8	1.4336
9	1.7075		9	1.3379
10	1.5605		10	1.2329
Mean 1.2809	Median 1.2742		Mean 1.2843	Median 1.3228
St. Dev. 0.3232	Var 0.1045		St. Dev. 0.1626	Var. 0.0264

A.11 3 lines $1mm$, $1.5mm$ & $2mm$ below Sample

A.11.1 No noise: 1.3008

A.11.2 1% noise

1% noise (95%)			1% noise (99.7%)	
Trial	Est. l		Trial	Est l
1	1.2832		1	1.2803
2	1.3125		2	1.3291
3	1.2827		3	1.3267
4	1.3672		4	1.2891
5	1.2227		5	1.2964
6	1.3311		6	1.3091
7	1.3047		7	1.3027
8	1.2695		8	1.2798
9	1.2651		9	1.3003
10	1.3525		10	1.2891
Mean 1.2991	Median 1.2939		Mean 1.3002	Median 1.2983
St. Dev. 0.0436	Var 0.0019		St. Dev. 0.0173	Var. $0.2997 * 10^{-3}$

A.11.3 5% noise

5% noise (95%)			5% noise (99.7%)	
Trial	Est. l		Trial	Est l
1	1.6182		1	1.2275
2	1.2520		2	1.5249
3	1.5283		3	1.3501
4	1.0972		4	1.4717
5	1.3384		5	1.3569
6	1.3560		6	1.3066
7	1.3799		7	1.4043
8	1.2817		8	1.3789
9	1.2441		9	1.0752
10	1.4599		10	1.3789
Mean 1.3555	Median 1.3472		Mean 1.3475	Median 1.3679
St. Dev. 0.1512	Var 0.0229		St. Dev. 0.1258	Var. 0.0158

B Results Varying the Length using A for the POD elements and B_1 in the Inverse Problem

B.1 1 line $1mm$ above Conducting Sheet

B.1.1 No noise: 1.2985

B.1.2 1% noise

1% noise (95%)			1% noise (99.7%)	
Trial	Est. l		Trial	Est l
1	1.2614		1	1.3666
2	1.4045		2	1.4433
3	1.1287		3	1.1973
4	1.3927		4	1.2750
5	1.8064		5	1.1771
6	1.1749		6	1.3930
7	1.0553		7	1.1605
8	1.2867		8	1.3307
9	1.4106		9	1.2473
10	1.0461		10	1.3660
Mean 1.2967	Median 1.2741		Mean 1.2957	Median 1.3028
St. Dev. 0.2258	Var 0.0510		St. Dev. 0.0985	Var. 0.0097

B.1.3 5% noise

5% noise (95%)			5% noise (99.7%)	
Trial	Est. l		Trial	Est l
1	0.6299		1	2.6106
2	1.6125		2	0.6149
3	0.6973		3	1.4914
4	0.5758		4	0.7580
5	0.1846		5	0.8566
6	2.4677		6	0.4537
7	0.0000		7	1.4921
8	0.5228		8	1.8085
9	0.4496		9	0.5834
10	0.0000		10	1.5533
Mean 0.7140	Median 0.5493		Mean 1.2223	Median 1.1743
St. Dev. 0.7685	Var 0.5906		St. Dev. 0.6866	Var. 0.4715

C Results Varying the Length using A for the POD elements and B_2 in the Inverse Problem

C.1 All of Ω

C.1.1 No noise: 1.3023

C.1.2 1% noise

1% noise (95%)			1% noise (99.7%)	
Trial	Est. l		Trial	Est l
1	1.3029		1	1.3028
2	1.3025		2	1.3024
3	1.3021		3	1.3027
4	1.3014		4	1.3024
5	1.3024		5	1.3021
6	1.3028		6	1.3021
7	1.3032		7	1.3024
8	1.3028		8	1.3026
9	1.3024		9	1.3023
10	1.3028		10	1.3022
Mean 1.3025	Median 1.3026		Mean 1.3024	Median 1.3024
St. Dev. $0.5057 * 10^{-3}$	Var $0.2558 * 10^{-6}$		St. Dev. $0.2355 * 10^{-3}$	Var. $0.5544 * 10^{-7}$

C.1.3 5% noise

5% noise (95%)			5% noise (99.7%)	
Trial	Est. l		Trial	Est l
1	1.3053		1	1.3021
2	1.3019		2	1.3015
3	1.3023		3	1.3021
4	1.3017		4	1.3031
5	1.2986		5	1.3035
6	1.3047		6	1.3014
7	1.3018		7	1.2978
8	1.3008		8	1.3037
9	1.3044		9	1.3047
10	1.3012		10	1.3030
Mean 1.3023	Median 1.3018		Mean 1.3023	Median 1.3025
St. Dev. 0.0020	Var $0.4472 * 10^{-5}$		St. Dev. 0.0019	Var. $0.3575 * 10^{-5}$

C.2 Air above Conducting Sheet

C.2.1 No noise: 1.2999

C.2.2 1% noise

1% noise (95%)			1% noise (99.7%)	
Trial	Est. l		Trial	Est l
1	1.3000		1	1.2998
2	1.2999		2	1.2999
3	1.2999		3	1.29998
4	1.3000		4	1.3000
5	1.2998		5	1.2998
6	1.2998		6	1.3000
7	1.3000		7	1.3000
8	1.3000		8	1.2999
9	1.2999		9	1.2997
10	1.2995		10	1.2999
Mean 1.2999	Median 1.2999		Mean 1.2999	Median 1.2999
St. Dev. $0.1629 * 10^{-3}$	Var $0.2653 * 10^{-7}$		St. Dev. $0.9256 * 10^{-4}$	Var. $0.8567 * 10^{-8}$

C.2.3 5% noise

5% noise (95%)			5% noise (99.7%)	
Trial	Est. l		Trial	Est l
1	1.2981		1	1.2998
2	1.3000		2	1.3002
3	1.3008		3	1.2993
4	1.2996		4	1.3003
5	1.2978		5	1.2995
6	1.2995		6	1.2995
7	1.3009		7	1.2995
8	1.2982		8	1.2995
9	1.2998		9	1.3006
10	1.2978		10	1.3006
Mean 1.2992	Median 1.2996		Mean 1.2999	Median 1.2997
St. Dev. 0.0012	Var $0.1426 * 10^{-5}$		St. Dev. $0.5727 * 10^{-3}$	Var. $0.3230 * 10^{-6}$

C.3 1 line $1mm$ above Conducting Sheet

C.3.1 No noise: 1.3011

C.3.2 1% noise

1% noise (95%)			1% noise (99.7%)	
Trial	Est. l		Trial	Est l
1	1.3009		1	1.3013
2	1.3013		2	1.3005
3	1.2989		3	1.3014
4	1.3015		4	1.3011
5	1.3022		5	1.3000
6	1.2993		6	1.3004
7	1.3014		7	1.3007
8	1.3007		8	1.3012
9	1.2998		9	1.3012
10	1.3018		10	1.3007
Mean 1.3008	Median 1.3011		Mean 1.3008	Median 1.3009
St. Dev. 0.0011	Var $0.1180 * 10^{-5}$		St. Dev. $0.4652 * 10^{-3}$	Var. $0.2165 * 10^{-6}$

C.3.3 5% noise

5% noise (95%)			5% noise (99.7%)	
Trial	Est. l		Trial	Est l
1	1.3024		1	1.3062
2	1.3021		2	1.3013
3	1.3068		3	1.3053
4	1.3000		4	1.3050
5	1.3001		5	1.2982
6	1.2969		6	1.2981
7	1.2985		7	1.3007
8	1.2992		8	1.2988
9	1.3032		9	1.3015
10	1.2926		10	1.2989
Mean 1.3002	Median 1.3000		Mean 1.3014	Median 1.3010
St. Dev. 0.0039	Var $0.1494 * 10^{-4}$		St. Dev. 0.0031	Var. $0.9653 * 10^{-5}$

10% **noise**

10% noise (95%)			10% noise (99.7%)	
Trial	Est. l		Trial	Est l
1	1.2981		1	1.2976
2	1.3090		2	1.3001
3	1.3072		3	1.3052
4	1.2983		4	1.3007
5	1.3092		5	1.2919
6	1.3023		6	1.3032
7	1.2944		7	1.2992
8	1.3065		8	1.2869
9	1.3090		9	1.3002
10	1.2962		10	1.2920
Mean 1.3030	Median 1.3044		Mean 1.2977	Median 1.2977
St. Dev. 0.0058	Var $0.3417 * 10^{-4}$		St. Dev. 0.0057	Var. $0.3237 * 10^{-4}$

C.4 2 lines $1mm$ & $1.5mm$ above Conducting Sheet

C.4.1 No noise: 1.3010

C.4.2 1% noise

1% noise (95%)			1% noise (99.7%)	
Trial	Est. l		Trial	Est l
1	1.3013		1	1.3011
2	1.3008		2	1.3010
3	1.3014		3	1.3017
4	1.3002		4	1.3006
5	1.3009		5	1.3012
6	1.3018		6	1.3005
7	1.3009		7	1.3009
8	1.3009		8	1.3009
9	1.3021		9	1.3006
10	1.3006		10	1.3017
Mean 1.3011	Median 1.3009		Mean 1.3010	Median 1.3009
St. Dev. $0.5835 * 10^{-3}$	Var $0.3403 * 10^{-6}$		St. Dev. $0.4109 * 10^{-3}$	Var. $0.1688 * 10^{-6}$

C.4.3 5% noise

5% noise (95%)			5% noise (99.7%)	
Trial	Est. l		Trial	Est l
1	1.3022		1	1.3031
2	1.3009		2	1.3016
3	1.3001		3	1.3027
4	1.2996		4	1.3024
5	1.2996		5	1.3024
6	1.3023		6	1.3004
7	1.3015		7	1.2995
8	1.3025		8	1.3003
9	1.3051		9	1.2959
10	1.3025		10	1.3002
Mean 1.3013	Median 1.3019		Mean 1.3008	Median 1.3010
St. Dev. 0.0023	Var $0.5150 * 10^{-5}$		St. Dev. 0.0021	Var. $0.4613 * 10^{-5}$

C.5 3 lines $1mm$, $1.5mm$ & $2mm$ above Conducting Sheet

C.5.1 No noise: 1.3010

C.5.2 1% noise

1% noise (95%)			1% noise (99.7%)	
Trial	Est. l		Trial	Est l
1	1.3017		1	1.3009
2	1.3015		2	1.3017
3	1.3011		3	1.3011
4	1.3012		4	1.3012
5	1.3005		5	1.3015
6	1.3015		6	1.3012
7	1.3005		7	1.3008
8	1.3013		8	1.3011
9	1.3010		9	1.3012
10	1.3015		10	1.3014
Mean 1.3012	Median 1.3013		Mean 1.3012	Median 1.3012
St. Dev. $0.4225 * 10^{-3}$	Var $0.1788 * 10^{-6}$		St. Dev. $0.2669 * 10^{-3}$	Var. $0.7123 * 10^{-7}$

C.5.3 5% noise

5% noise (95%)			5% noise (99.7%)	
Trial	Est. l		Trial	Est l
1	1.3034		1	1.3036
2	1.2988		2	1.3005
3	1.3043		3	1.2989
4	1.2983		4	1.2994
5	1.3035		5	1.3013
6	1.3042		6	1.3040
7	1.2961		7	1.2954
8	1.2994		8	1.2989
9	1.3059		9	1.2979
10	1.3030		10	1.3022
Mean 1.3017	Median 1.3032		Mean 1.3002	Median 1.2999
St. Dev. 0.0033	Var $0.1059 * 10^{-4}$		St. Dev. 0.0027	Var. $0.7077 * 10^{-5}$

C.6 Air below Sample

C.6.1 No noise: 1.3012

C.6.2 1% noise

1% noise (95%)			1% noise (99.7%)	
Trial	Est. l		Trial	Est l
1	1.3010		1	1.3013
2	1.3012		2	1.3011
3	1.3012		3	1.3009
4	1.3010		4	1.3010
5	1.3013		5	1.3011
6	1.3010		6	1.3014
7	1.3015		7	1.3013
8	1.3014		8	1.3013
9	1.3009		9	1.3011
10	1.3009		10	1.3014
Mean 1.3012	Median 1.3011		Mean 1.3012	Median 1.3012
St. Dev. $0.2175 * 10^{-3}$	Var $0.4730 * 10^{-7}$		St. Dev. $0.1596 * 10^{-3}$	Var. $0.2548 * 10^{-7}$

C.6.3 5% noise

5% noise (95%)			5% noise (99.7%)	
Trial	Est. l		Trial	Est l
1	1.3024		1	1.3024
2	1.3017		2	1.3015
3	1.2999		3	1.3020
4	1.2990		4	1.3006
5	1.3016		5	1.3003
6	1.3011		6	1.3020
7	1.2995		7	1.3021
8	1.3026		8	1.3002
9	1.2990		9	1.3012
10	1.3012		10	1.3016
Mean 1.3007	Median 1.3006		Mean 1.3014	Median 1.3015
St. Dev. 0.0014	Var $0.1848 * 10^{-5}$		St. Dev. $0.7194 * 10^{-3}$	Var. $0.5176 * 10^{-6}$

C.7 1 line $1mm$ below Sample

C.7.1 No noise: 1.3014

C.7.2 1% noise

1% noise (95%)			1% noise (99.7%)	
Trial	Est. l		Trial	Est l
1	1.3007		1	1.3011
2	1.3025		2	1.3018
3	1.3032		3	1.3019
4	1.3003		4	1.3018
5	1.3003		5	1.3028
6	1.3014		6	1.3004
7	1.3019		7	1.3013
8	1.3016		8	1.3012
9	1.3024		9	1.3019
10	1.3025		10	1.3010
Mean 1.3017	Median 1.3017		Mean 1.3015	Median 1.3015
St. Dev. $0.9441 * 10^{-3}$	Var $0.8914 * 10^{-6}$		St. Dev. $0.6565 * 10^{-3}$	Var. $0.4309 * 10^{-6}$

C.7.3 5% noise

5% noise (95%)			5% noise (99.7%)	
Trial	Est. l		Trial	Est l
1	1.2972		1	1.3060
2	1.2992		2	1.3016
3	1.3047		3	1.3006
4	1.3052		4	1.2943
5	1.3040		5	1.3024
6	1.3045		6	1.3020
7	1.3056		7	1.2941
8	1.3021		8	1.2996
9	1.3026		9	1.3021
10	1.2927		10	1.3006
Mean 1.3018	Median 1.3033		Mean 1.3003	Median 1.3011
St. Dev. 0.0042	Var $0.1763 * 10^{-4}$		St. Dev. 0.0036	Var. $0.1324 * 10^{-4}$

10% **noise**

10% noise (95%)			10% noise (99.7%)	
Trial	Est. l		Trial	Est l
1	1.3148		1	1.3015
2	1.3017		2	1.3000
3	1.2986		3	1.3043
4	1.2796		4	1.3115
5	1.3039		5	1.3012
6	1.3029		6	1.3136
7	1.2792		7	1.3117
8	1.2955		8	1.2911
9	1.3033		9	1.2997
10	1.2986		10	1.3041
Mean 1.2978	Median 1.3001		Mean 1.3039	Median 1.3028
St. Dev. 0.0110	Var $0.1203 * 10^{-3}$		St. Dev. 0.0068	Var. $0.4681 * 10^{-4}$

C.8 2 lines $1mm$ & $1.5mm$ below Sample

C.8.1 No noise: 1.3015

C.8.2 1% noise

1% noise (95%)			1% noise (99.7%)	
Trial	Est. l		Trial	Est l
1	1.3011		1	1.3013
2	1.3015		2	1.3016
3	1.3011		3	1.3011
4	1.3028		4	1.3017
5	1.3022		5	1.3010
6	1.3029		6	1.3023
7	1.3020		7	1.3022
8	1.3003		8	1.3015
9	1.3010		9	1.3011
10	1.3017		10	1.3020
Mean 1.3017	Median 1.3016		Mean 1.3016	Median 1.3016
St. Dev. $0.8305 * 10^{-3}$	Var $0.6898 * 10^{-6}$		St. Dev. $0.4699 * 10^{-3}$	Var. $0.2208 * 10^{-6}$

C.8.3 5% noise

5% noise (95%)			5% noise (99.7%)	
Trial	Est. l		Trial	Est l
1	1.3030		1	1.3036
2	1.3000		2	1.2994
3	1.3081		3	1.3036
4	1.3018		4	1.2961
5	1.2995		5	1.3026
6	1.3011		6	1.3029
7	1.3029		7	1.3025
8	1.3034		8	1.3025
9	1.3005		9	1.3013
10	1.3076		10	1.3026
Mean 1.3028	Median 1.3023		Mean 1.3017	Median 1.3025
St. Dev. 0.0030	Var $0.8803 * 10^{-5}$		St. Dev. 0.0023	Var. $0.5309 * 10^{-5}$

C.9 3 lines $1mm$, $1.5mm$ & $2mm$ below Sample

C.9.1 No noise: 1.3010

C.9.2 1% noise

1% noise (95%)			1% noise (99.7%)	
Trial	Est. l		Trial	Est l
1	1.3010		1	1.3011
2	1.3020		2	1.3010
3	1.3012		3	1.3010
4	1.3014		4	1.3020
5	1.3014		5	1.3013
6	1.3009		6	1.3018
7	1.3018		7	1.3014
8	1.3013		8	1.3008
9	1.2998		9	1.3005
10	1.3013		10	1.3013
Mean 1.3012	Median 1.3013		Mean 1.3012	Median 1.3012
St. Dev. $0.6024 * 10^{-3}$	Var $0.3628 * 10^{-6}$		St. Dev. $0.4514 * 10^{-3}$	Var. $0.2038 * 10^{-6}$

C.9.3 5% noise

5% noise (95%)			5% noise (99.7%)	
Trial	Est. l		Trial	Est l
1	1.3000		1	1.3008
2	1.2986		2	1.2998
3	1.2940		3	1.3005
4	1.3042		4	1.3025
5	1.3047		5	1.2995
6	1.3018		6	1.2961
7	1.2993		7	1.2993
8	1.3045		8	1.3035
9	1.3036		9	1.3025
10	1.3055		10	1.3035
Mean 1.3016	Median 1.3027		Mean 1.3003	Median 1.3007
St. Dev. 0.0037	Var $0.1345 * 10^{-4}$		St. Dev. 0.0023	Var. $0.5295 * 10^{-5}$

D Results Varying the Length using B_2 for the POD elements and $B2$ in the Inverse Problem

D.1 1 line $1mm$ above Conducting Sheet

D.1.1 No noise: 1.2978

D.1.2 1% noise

1% noise (95%)			1% noise (99.7%)	
Trial	Est. l		Trial	Est l
1	1.2974		1	1.2955
2	1.2974		2	1.2977
3	1.3001		3	1.2974
4	1.2981		4	1.2981
5	1.2976		5	1.2981
6	1.2975		6	1.2979
7	1.2970		7	1.2974
8	1.2977		8	1.2977
9	1.2980		9	1.2982
10	1.2993		10	1.2977
Mean 1.2980	Median 1.2977		Mean 1.2976	Median 1.2977
St. Dev. $0.9590 * 10^{-3}$	Var $0.9197 * 10^{-6}$		St. Dev. $0.7898 * 10^{-3}$	Var. $0.6237 * 10^{-6}$

D.1.3 5% noise

5% noise (95%)			5% noise (99.7%)	
Trial	Est. l		Trial	Est l
1	1.2909		1	1.3028
2	1.2993		2	1.3013
3	1.2964		3	1.2970
4	1.2872		4	1.2965
5	1.2971		5	1.2996
6	1.2910		6	1.3018
7	1.2940		7	1.3060
8	1.2940		8	1.2996
9	1.2969		9	1.2958
10	1.3056		10	1.2984
Mean 1.2952	Median 1.2952		Mean 1.2999	Median 1.2999
St. Dev. 0.0051	Var $0.2631 * 10^{-4}$		St. Dev. 0.0032	Var. $0.1017 * 10^{-4}$

D.2 2 lines $1mm$ & $1.5mm$ above Conducting Sheet

D.2.1 No noise: 1.2978

D.2.2 1% noise

1% noise (95%)			1% noise (99.7%)	
Trial	Est. l		Trial	Est l
1	1.2981		1	1.2980
2	1.2977		2	1.2977
3	1.2976		3	1.2976
4	1.2990		4	1.2980
5	1.2978		5	1.2978
6	1.2992		6	1.2969
7	1.2984		7	1.2975
8	1.2980		8	1.2982
9	1.2987		9	1.2981
10	1.2964		10	1.2974
Mean 1.2981	Median 1.2980		Mean 1.2977	Median 1.2977
St. Dev. $0.8098 * 10^{-3}$	Var $0.6558 * 10^{-6}$		St. Dev. $0.3959 * 10^{-3}$	Var. $0.1592 * 10^{-6}$

D.2.3 5% noise

5% noise (95%)			5% noise (99.7%)	
Trial	Est. l		Trial	Est l
1	1.2987		1	1.2988
2	1.2942		2	1.2989
3	1.2985		3	1.3011
4	1.2931		4	1.2981
5	1.2988		5	1.2979
6	1.2988		6	1.2990
7	1.3021		7	1.2997
8	1.2957		8	1.2970
9	1.3026		9	1.2940
10	1.2942		10	1.2969
Mean 1.2977	Median 1.2986		Mean 1.2981	Median 1.2984
St. Dev. 0.0033	Var $0.1079 * 10^{-4}$		St. Dev. 0.0019	Var. $0.3638 * 10^{-5}$

D.3 1 line $1mm$ below Sample

D.3.1 No noise: 1.2974

D.3.2 1% noise

1% noise (95%)			1% noise (99.7%)	
Trial	Est. l		Trial	Est l
1	1.2970		1	1.2982
2	1.2982		2	1.2978
3	1.2975		3	1.2985
4	1.2981		4	1.2966
5	1.2962		5	1.2987
6	1.2957		6	1.2970
7	1.2973		7	1.2990
8	1.2979		8	1.2975
9	1.2964		9	1.2985
10	1.2981		10	1.2971
Mean 1.2972	Median 1.2972		Mean 1.2979	Median 1.2980
St. Dev. $0.9133 * 10^{-3}$	Var $0.8340 * 10^{-6}$		St. Dev. $0.8261 * 10^{-3}$	Var. $0.6824 * 10^{-6}$

D.3.3 5% noise

5% noise (95%)			5% noise (99.7%)	
Trial	Est. l		Trial	Est l
1	1.2971		1	1.2986
2	1.2990		2	1.2992
3	1.2970		3	1.3013
4	1.2998		4	1.3026
5	1.2959		5	1.3000
6	1.3086		6	1.2963
7	1.2968		7	1.2956
8	1.2987		8	1.2959
9	1.2934		9	1.2997
10	1.2985		10	1.2973
Mean 1.2985	Median 1.2978		Mean 1.2986	Median 1.2989
St. Dev. 0.0040	Var $0.1597 * 10^{-4}$		St. Dev. 0.0024	Var. $0.5578 * 10^{-5}$

D.4 2 lines $1mm$ & $1.5mm$ below Sample

D.4.1 No noise: 1.2974

D.4.2 1% noise

1% noise (95%)			1% noise (99.7%)	
Trial	Est. l		Trial	Est l
1	1.2966		1	1.2979
2	1.2983		2	1.2971
3	1.2972		3	1.2982
4	1.2975		4	1.2979
5	1.2984		5	1.2973
6	1.2975		6	1.2980
7	1.2976		7	1.2970
8	1.2982		8	1.2975
9	1.2980		9	1.2974
10	1.2971		10	1.2977
Mean 1.2977	Median 1.2976		Mean 1.2976	Median 1.2976
St. Dev. $0.5815 * 10^{-3}$	Var $0.3382 * 10^{-6}$		St. Dev. $0.3915 * 10^{-3}$	Var. $0.1533 * 10^{-6}$

D.4.3 5% noise

5% noise (95%)			5% noise (99.7%)	
Trial	Est. l		Trial	Est l
1	1.2926		1	1.2978
2	1.3006		2	1.2995
3	1.3035		3	1.2947
4	1.2924		4	1.2990
5	1.2969		5	1.3002
6	1.2966		6	1.2978
7	1.2950		7	1.2990
8	1.2980		8	1.2961
9	1.2989		9	1.3006
10	1.3004		10	1.3001
Mean 1.2975	Median 1.2975		Mean 1.2985	Median 1.2990
St. Dev. 0.0035	Var $0.1254 * 10^{-4}$		St. Dev. 0.0019	Var. $0.3592 * 10^{-5}$

E Results Varying the Thickness using A for the POD elements and B_2 in the Inverse Problem

E.1 1 line $1mm$ above Conducting Sheet

E.1.1 No noise: 1.3036

E.1.2 1% noise

1% noise (95%)			1% noise (99.7%)	
Trial	Est. h		Trial	Est h
1	1.3052		1	1.3035
2	1.3045		2	1.3039
3	1.3042		3	1.3038
4	1.3027		4	1.3037
5	1.3033		5	1.3034
6	1.3036		6	1.3043
7	1.3025		7	1.3041
8	1.3030		8	1.3031
9	1.3045		9	1.3033
10	1.3050		10	1.3047
Mean 1.3037	Median 1.3035		Mean 1.3038	Median 1.3037
St. Dev. $0.8351 * 10^{-3}$	Var $0.6974 * 10^{-6}$		St. Dev. $0.4875 * 10^{-3}$	Var. $0.2377 * 10^{-6}$

E.1.3 5% noise

5% noise (95%)			5% noise (99.7%)	
Trial	Est. h		Trial	Est h
1	1.3032		1	1.3070
2	1.3053		2	1.3072
3	1.3022		3	1.3022
4	1.3011		4	1.3063
5	1.2987		5	1.3056
6	1.3030		6	1.3006
7	1.3013		7	1.3026
8	1.3054		8	1.3035
9	1.3102		9	1.2999
10	1.3045		10	1.3015
Mean 1.3035	Median 1.3031		Mean 1.3036	Median 1.3031
St. Dev. 0.0031	Var $0.9847 * 10^{-5}$		St. Dev. 0.0027	Var. $0.7377 * 10^{-5}$

10% **noise**

10% noise (95%)			10% noise (99.7%)	
Trial	Est. h		Trial	Est h
1	1.2098		1	1.3058
2	1.2928		2	1.3069
3	1.3087		3	1.3124
4	1.2952		4	1.2952
5	1.3008		5	1.3072
6	1.3144		6	1.3054
7	1.3080		7	1.2997
8	1.3047		8	1.3024
9	1.3166		9	1.2973
10	1.3050		10	1.3087
Mean	Median		Mean	Median
1.3037	1.3049		1.3041	1.3056
St. Dev.	Var		St. Dev.	Var.
0.0088	$0.7716 * 10^{-4}$		0.0054	$0.2883 * 10^{-4}$

E.2 2 lines $1mm$ & $1.5mm$ above Conducting Sheet

E.2.1 No noise: 1.3046

E.2.2 1% noise

1% noise (95%)			1% noise (99.7%)	
Trial	Est. h		Trial	Est h
1	1.3043		1	1.3040
2	1.3049		2	1.3043
3	1.3046		3	1.3051
4	1.3056		4	1.3046
5	1.3020		5	1.3039
6	1.3043		6	1.3051
7	1.3035		7	1.3042
8	1.3054		8	1.3042
9	1.3039		9	1.3049
10	1.3052		10	1.3042
Mean 1.3044	Median 1.3045		Mean 1.3044	Median 1.3042
St. Dev. 0.0011	Var $0.1112 * 10^{-5}$		St. Dev. $0.4425 * 10^{-3}$	Var. $0.1988 * 10^{-6}$

E.2.3 5% noise

5% noise (95%)			5% noise (99.7%)	
Trial	Est. h		Trial	Est h
1	1.2983		1	1.3083
2	1.3011		2	1.3057
3	1.3061		3	1.3038
4	1.3094		4	1.3052
5	1.3063		5	1.3041
6	1.3098		6	1.3042
7	1.3038		7	1.3036
8	1.3032		8	1.3071
9	1.3070		9	1.3049
10	1.3103		10	1.3085
Mean 1.3055	Median 1.3062		Mean 1.3055	Median 1.3051
St. Dev. 0.0039	Var $0.1543 * 10^{-4}$		St. Dev. 0.0018	Var. $0.3296 * 10^{-5}$

E.3 1 line $1mm$ below Sample

E.3.1 No noise: 1.2997

E.3.2 1% noise

1% noise (95%)			1% noise (99.7%)	
Trial	Est. h		Trial	Est h
1	1.2999		1	1.3002
2	1.3015		2	1.3000
3	1.2980		3	1.3000
4	1.2992		4	1.3002
5	1.2990		5	1.2998
6	1.3000		6	1.2998
7	1.2988		7	1.2985
8	1.2989		8	1.3005
9	1.2991		9	1.2997
10	1.3002		10	1.2995
Mean 1.2995	Median 1.2992		Mean 1.2998	Median 1.2999
St. Dev. $0.9643 * 10^{-3}$	Var $0.9298 * 10^{-6}$		St. Dev. $0.5376 * 10^{-3}$	Var. $0.2890 * 10^{-6}$

E.3.3 5% noise

5% noise (95%)			5% noise (99.7%)	
Trial	Est. h		Trial	Est h
1	1.2888		1	1.3042
2	1.3002		2	1.2995
3	1.2998		3	1.3055
4	1.2889		4	1.3048
5	1.2962		5	1.2940
6	1.3004		6	1.2988
7	1.2988		7	1.3003
8	1.2997		8	1.2954
9	1.2985		9	1.3041
10	1.3023		10	1.2968
Mean 1.2974	Median 1.2993		Mean 1.3003	Median 1.2999
St. Dev. 0.0047	Var $0.2237 * 10^{-4}$		St. Dev. 0.0041	Var. $0.1718 * 10^{-4}$

10% **noise**

10% noise (95%)			10% noise (99.7%)	
Trial	Est. h		Trial	Est h
1	1.2919		1	1.2952
2	1.2941		2	1.3023
3	1.3054		3	1.3030
4	1.3072		4	1.3010
5	1.3048		5	1.3114
6	1.3046		6	1.2886
7	1.3071		7	1.2967
8	1.3011		8	1.2955
9	1.3014		9	1.3019
10	1.2820		10	1.2940
Mean 1.3000	Median 1.3030		Mean 1.2989	Median 1.2988
St. Dev. 0.0082	Var $0.6733 * 10^{-4}$		St. Dev. 0.0063	Var. $0.3986 * 10^{-4}$

E.4 2 lines $1mm$ & $1.5mm$ below Sample

E.4.1 No noise: 1.2998

E.4.2 1% noise

1% noise (95%)			1% noise (99.7%)	
Trial	Est. h		Trial	Est h
1	1.2999		1	1.2998
2	1.2988		2	1.2996
3	1.3008		3	1.2997
4	1.3007		4	1.3000
5	1.2997		5	1.3001
6	1.2990		6	1.2997
7	1.3003		7	1.3006
8	1.3001		8	1.3002
9	1.2995		9	1.2994
10	1.3011		10	1.3002
Mean 1.3000	Median 1.3000		Mean 1.2999	Median 1.2999
St. Dev. $0.7593 * 10^{-3}$	Var $0.5765 * 10^{-6}$		St. Dev. $0.3458 * 10^{-3}$	Var. $0.1196 * 10^{-6}$

E.4.3 5% noise

5% noise (95%)			5% noise (99.7%)	
Trial	Est. h		Trial	Est h
1	1.2914		1	1.3012
2	1.3014		2	1.2998
3	1.3016		3	1.2965
4	1.3006		4	1.3037
5	1.3007		5	1.3005
6	1.2993		6	1.2939
7	1.3012		7	1.2995
8	1.2994		8	1.2986
9	1.3057		9	1.3006
10	1.2994		10	1.2988
Mean 1.3001	Median 1.3007		Mean 1.2993	Median 1.2997
St. Dev. 0.0036	Var $0.1262 * 10^{-4}$		St. Dev. 0.0027	Var. $0.7071 * 10^{-5}$